Topological Protection Can Arise from Thermal Fluctuations and Interactions

Ricardo Pablo Pedro, Jayson Paulose, Anton Souslov, Mildred Dresselhaus, and Vincenzo Vitelli

Topological protection can arise from thermal fluctuations and interactions

Ricardo Pablo Pedro,[1, *] Jayson Paulose,[2, *] Anton Souslov,[3, 4] Mildred Dresselhaus,[5] and Vincenzo Vitelli[3, †]

[1]*Department of Chemistry, Massachusetts Institute of Technology, Cambridge, MA 02139, USA*
[2]*Department of Physics and Institute of Theoretical Science, University of Oregon, Eugene, OR 97403, USA*
[3]*The James Franck Institute and Department of Physics,*
The University of Chicago, Chicago, IL 60637, USA
[4]*Department of Physics, University of Bath, Bath BA2 7AY, United Kingdom*
[5]*Department of Physics and Department of Electrical Engineering and Computer Science,*
Massachusetts Institute of Technology, Cambridge, MA 02139, USA

Topological quantum and classical materials can exhibit robust properties that are protected against disorder, for example for noninteracting particles and linear waves. Here, we demonstrate how to construct topologically protected states that arise from the combination of strong interactions and thermal fluctuations inherent to soft materials or miniaturized mechanical structures. Specifically, we consider fluctuating lines under tension (e.g., polymer or vortex lines), subject to a class of spatially modulated substrate potentials. At equilibrium, the lines acquire a collective tilt proportional to an integer topological invariant called the Chern number. This quantized tilt is robust against substrate disorder, as verified by classical Langevin dynamics simulations. This robustness arises because excitations in this system of thermally fluctuating lines are gapped by virtue of inter-line interactions. We establish the topological underpinning of this pattern via a mapping that we develop between the interacting-lines system and a hitherto unexplored generalization of Thouless pumping to imaginary time. Our work points to a new class of classical topological phenomena in which the topological signature manifests itself in a structural property observed at finite temperature rather than a transport measurement.

Topological mechanics [1–6] and optics [7, 8] typically focus on systems of linear waves assuming that mode interactions and finite-temperature effects can be ignored in deriving the relevant topological invariants and corresponding physical observables. However, these assumptions break-down when structures are miniaturized down to the micron scale. The resulting interplay between large-amplitude thermal displacements and mechanical constraints arises in contexts ranging from molecular robotics to soft materials. In this Letter, we show that thermal fluctuations and interactions, far from being a hindrance, can actually create topologically protected states by acting in tandem. We provide a specific illustration of this mechanism in thermally fluctuating and interacting lines (or chains) under tension whose statistics describe such diverse systems as directed polymers [9–12] and vortex lines in superconductors [13, 14].

Consider, as an example, flexible lines confined within a thin layer parallel to the xy–plane and experiencing a tension τ along the direction y (Fig. 1a). The lines undergo thermal fluctuations along the x direction but are assumed to be inextensible along the longitudinal direction. Spatial modulations in the polymer-substrate interaction potential influence the line density profile at equilibrium (Fig. 1b). Previous studies of directed-line systems have focused on the effect of localized or randomly-distributed constraining potentials on line conformations [13, 15]. By contrast, we characterize the patterns induced by *periodic* substrate potentials. Although the underlying principle is more general, we focus here on the specific form for the potential energy per unit length [16, 17]

$$V(x,y) = V_1 \cos\left(\frac{2\pi q}{a}x\right) + V_2 \cos\left(\frac{2\pi p}{a}x - \frac{2\pi}{\lambda}y\right), \ (1)$$

which combines a y-independent sinusoidal component (first term) with a mixed one (second term) which slides along the x-direction as y advances (Fig. 1c). The period in the x–direction is given by a divided by the greatest common divisor of the integers p and q, and in the y–direction the period is denoted by λ. (V_1 and V_2 set the strength of the substrate interaction per unit length of the chains.) The form of the potential in Eq. (1) is motivated by an analogy between the system of fluctuating lines and the so-called Thouless charge pump [18], which was recently realized and extended in ultracold atom experiments [19–21]. As we shall see, the formalism of the Thouless pump needs to be extended to account for the thermally fluctuating classical systems considered here.

A quantum Thouless pump describes the adiabatic flow of charge in a one-dimensional electron gas subject to a potential that varies periodically in both space and time. When the electrons populate an energy band completely, the number of electrons transported in one cycle is quantized to an integer-valued topological invariant of the filled band—the Chern number, $\mathcal{C}$ [22]. The static potential in Eq. 1 can be viewed as a time-dependent potential with the spatial coordinate y interpreted as the time coordinate. For electrons experiencing this potential, the Chern numbers are determined by the integers p and q [23] and can be nonzero, leading to charge flow. For the potential in Fig. 1 with $(p, q) = (1, 2)$, the lowest band has $\mathcal{C} = 1$. Hence, under a filling density of one
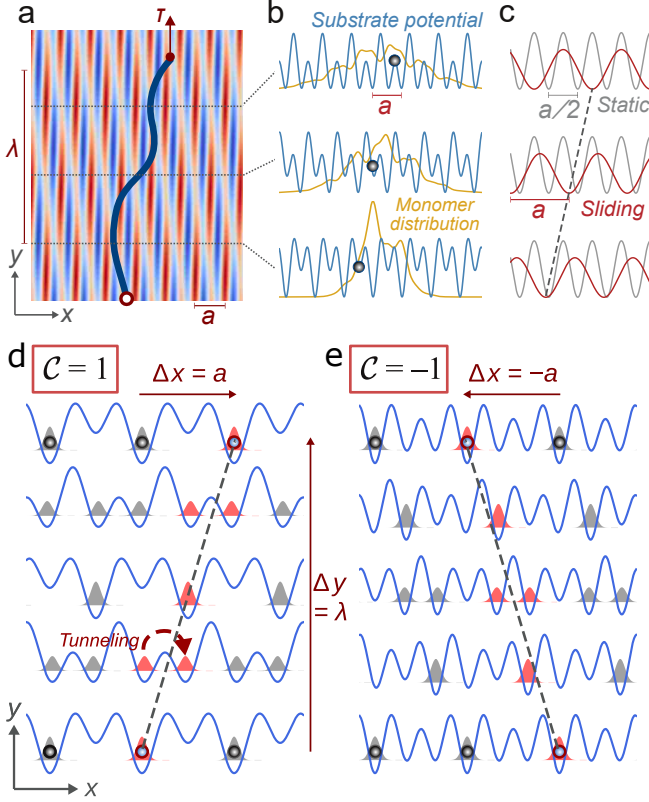
FIG. 1. **Directed lines and doubly-periodic substrate potentials.** (a) Schematic of single directed line in a potential described by Eq. (1) with $(p, q) = (1, 2)$, y-axis period λ, and x-axis period a. (b) Substrate potential (blue curves) and the theoretical density distribution [from Eq. (2), yellow curves] for a single chain at three y-positions indicated by the dotted lines. (c) The compound potential $V(x, y)$ [blue] combines two components, static (gray) with wavelength $a/q = a/2$ and sliding (red) with wavelength $a/p = a$. (d) Illustration of a Thouless pump for a potential with $(p, q) = (1, 2)$, corresponding to $\mathcal{C} = 1$. Under a filling density of one electron per lattice constant, each electron is exponentially localized to a unique unit cell. The drift of one such localized wavefunction over an adiabatic cycle is shown schematically; it is exactly quantized to $\mathcal{C}$ steps of lattice size a over each period λ of the potential variation along the y direction. The tunneling of probability weight between adjacent potential minima during the adiabatic evolution, indicated by the dashed arrow, is crucial for the shift. (e) Same as (d) for a potential with $(p, q) = (2, 3)$ for which $\mathcal{C} = -1$.

electron per lattice period a, the electrons are shifted to the *right* by one lattice period over one time cycle λ, see Fig. 1d. By contrast, Fig. 1e illustrates the case $(p, q) = (2, 3)$, for which $\mathcal{C} = -1$. In this case of so-called "anomalous" pumping [17], the electrons flow to the *left* even though the potential is still sliding to the right. As long as the gap between occupied and unoccupied bands remains open, the topological nature of $\mathcal{C}$ insures that the charge flow is robust against electron interactions and disorder in the potential $V(x, y)$ [24].

Can we formulate a thermal generalization of Thouless pumping and use it to engineer topological soft materials? Here, we show that directed fluctuating lines can order into tilted patterns that mimic the spacetime paths traced by the quantum particles in Fig. 1d–e. Several studies have shown that the conformations of a thermally fluctuating chain can be mapped to the paths of a quantum particle [9–12, 25, 26]. However, Thouless pumping introduces a new facet to this mapping: the requirement of a gapped phase. For electrons, the gapped phase is accomplished by filling a band, which requires Pauli exclusion—a distinctive feature of fermions. To recreate exclusion effects in classical fluctuating lines, we impose a requirement that lines cannot cross each other. Such a constraint could be the result of simple steric exclusion between lines made of freely-jointed rigid elements, or of screened repulsive interactions that act at very short distances. Remarkably, the noncrossing constraint reproduces the effects of Fermi statistics in the directed line system [9], allowing us to "fill" bands by tuning the number of chains per lattice constant along the x-direction.

To test whether interacting, thermal chains can replicate topological charge pumping, we have conducted Langevin dynamics simulations [27] of chains of monomers interacting with each other via a harmonic contact repulsion below a cutoff separation and, in addition, interacting with the substrate according to Eq. (1) with $V_1 a$ and $V_2 a$ of the same order as the thermal energy $k_B T$. We emulate filling of the lowest band by including lines at a density of one chain per lattice constant a. When parameters $(p, q) = (1, 2)$ are chosen so that $\mathcal{C} = 1$, the chains acquire a collective tilt to the right (Fig. 2a) which is also apparent in the equilibrium density profile (Fig. 2b). Probability distributions of the monomer x-positions at different values of y show that the shift in average chain position advances to the right by one lattice constant per cycle, matching the quantization expected from the Chern number to within 1% accuracy (Figs. 2c–d).

In contrast to the quantum pump, the topological tilt of the lines is a direct consequence of many-body interactions between the chains: a single chain on an otherwise empty lattice diffuses freely through the system and, on average, does not tilt (see Supplemental Movies 1–3 [27]). Moreover, thermal fluctuations do not destroy the topological state, but rather are crucial for creating the tilt via a series of "thermal tunneling" events visible in the density profiles of Fig. 2c (see also Supplemental Figure 2 [27]). These events are analogous to the quantum tunneling in Fig. 1.

The non-vanishing slope resulting whenever $\mathcal{C} \neq 0$ cannot be intuited from superficial aspects of the substrate potential or from the (real-time) dynamics of classical particles under the same potential (see Supplemental Figure 2 [27] for a comparison of the classical path to the true contour at thermal equilibrium, which highlights the role
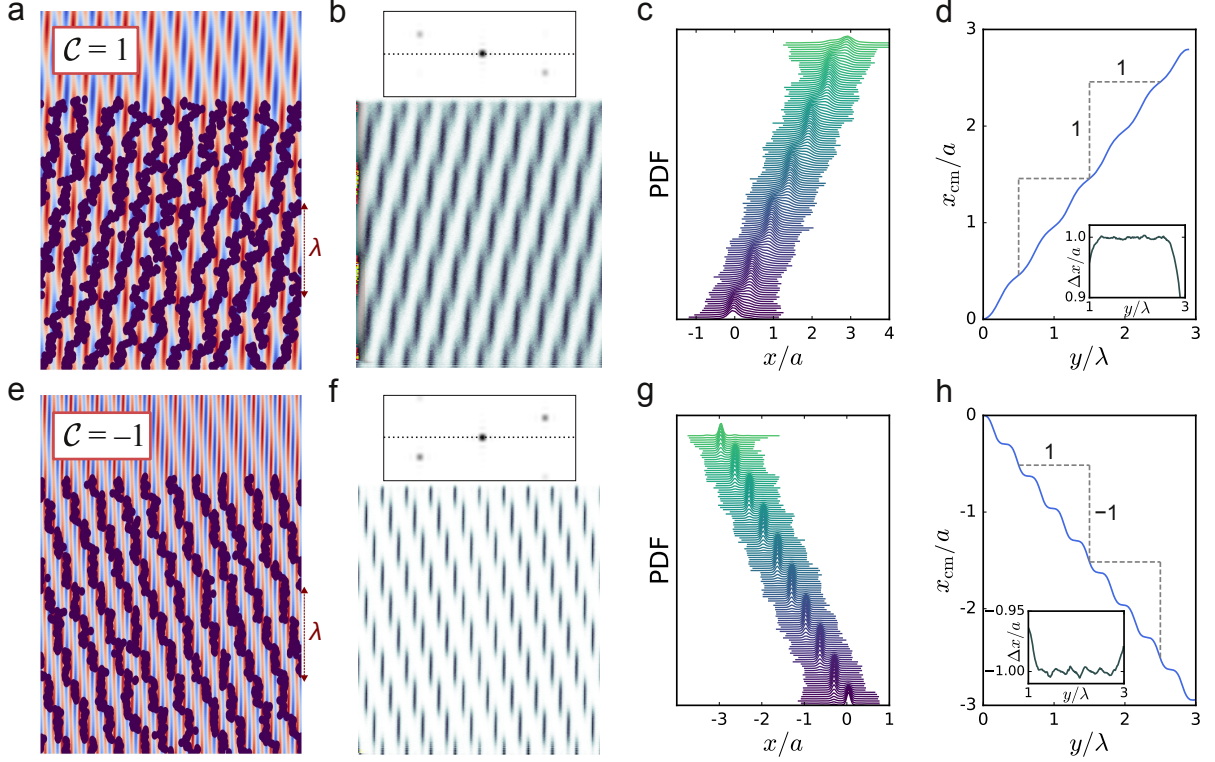
FIG. 2. **Topological tilt of directed line conformations. a,** Snapshot of a molecular dynamics simulation [27] of ten noncrossing directed lines experiencing the substrate potential from Fig. 2a with $\mathcal{C} = 1$ under commensurate filling (one chain per unit cell of the potential along the x direction). **b,** Equilibrium monomer density distribution, and numerically-computed scattering intensity profile (inset; see Methods). **c,** Probability distribution of monomer x-position for a subset of monomers along the length of the chains. Data from different chains are aggregated by first shifting the pth chain by an amount pa along x, where $p \in \{0, ..., 9\}$ indexes the chains in order from left to right. **d,** Centre of mass computed from the probability distributions in **c**. The inset shows the shift over one period, $x_{\mathrm{cm}}(y) - x_{\mathrm{cm}}(y - \lambda)$, which agrees with the prediction of $\mathcal{C} = 1$ away from the line ends. **e–h,** Same as **a–d** for the potential from Fig. 2b with $\mathcal{C} = -1$. The lines display an anomalous tilt to the left, even though the potential slides to the right with increasing y.

of the thermal tunneling events in producing the tilt). For instance, Fig. 2e–h shows the case $(p, q) = (2, 3)$, for which $\mathcal{C} = -1$. Surprisingly, the lines tilt to the left even though the sliding part of the potential, given by the last term in Eq. (1), has the positive slope $a/(\lambda p)$ which by itself would suggest a tilt to the right. Note that the topologically distinct left- and right-leaning configurations can be differentiated by their diffraction patterns (Figs. 2b and 2f, insets), suggesting a scattering experiment that would directly measure the underlying topological index.

To rigorously establish the topological origin of the observed tilt, we turn to the aforementioned mathematical correspondence between quantum particles and thermally fluctuating lines[9–12, 25, 26, 34–36]. This quantum-classical correspondence stems from the formal similarity between the Schrödinger equation and the diffusion equation describing the chain statistics:

$$\partial_y \Psi = \frac{k_B T}{2\tau} \partial_x^2 \Psi - \frac{1}{k_B T} V \Psi \equiv H \Psi. \qquad (2)$$

Interpreted using the directed line language, Eq. (2) describes the (real) probability distribution $\Psi(x, y)$ of chain location x at distance y from the constrained end at $y = 0$, given the initial distribution $\Psi(x, 0)$. [The external tension prevents directed chains from doubling back on themselves, which means that the instantaneous chain configurations are described by single-valued functions $x(y)$.] On the other hand, upon equating y with it and $k_B T$ with $\hbar$, Eq. (2) describes the evolution of the (complex) wavefunction $\Psi(x, t)$ for a particle of mass τ in the time-dependent potential $V(x, t)$. The transformation to imaginary time is a key aspect of our proposal in two ways. First, it guarantees that the solutions to Eq. (2) for long chains are described by the ground-state wavefunction of the analogous quantum system [27]. Below we exploit this condition, known as *ground-state dominance*, to generate a gapped state. Going to imaginary time also turns wavelike Bloch eigenstates into eigenstates that decay with propagation, and thus requires an extension of the standard formalism of Thouless pumping beyond the quantum case which we perform later on.

Inter-line interactions, together with ground-state dominance, can give rise to gapped phases. To see this, consider the y-evolution of the joint probability distribution of x-positions $\{x_0(y), x_1(y), ..., x_N(y)\}$ of N chains in a y-*independent* potential $V(x)$, such as the potential in Eq. (1) when $V_2 = 0$. This many-body probability is described via the exchange-symmetric eigenstates of the effective Hamiltonian H in Eq. (2), augmented by a pair interaction term of the form $(k_B T)^{-1} \sum_{i<j} V_p(x_i - x_j)$. These (bosonic) many-body eigenstates may be challenging to describe. However, a tremendous simplification exists for non-crossing directed lines, for which the pair potential is infinitely large when the positions of two lines coincide at any y and is zero otherwise: $V_p = c\delta(x_i - x_j)$, $c \to \infty$. In this case, there is a one-to-one mapping between the requisite exchange-symmetric line eigenstates and the many-body wavefunctions of N noninteracting *fermions* confined to the x–axis and experiencing the same substrate potential $V(x)$ [9, 37]. In particular, if the number of lines is equal to the number of lattice periods, the ground state is obtained by filling up the lowest band entirely. This trivial electronic insulator in the fermion picture describes a Mott insulator in the fluctuating-line picture [27]: a state in which excitations are gapped by virtue of interactions. Up to an overall normalization, the many-body joint probability distribution of the line system Ψ_0^P is then equal to the *absolute value* of the fermionic ground state Ψ_0^F [9, 12, 37].

When this gapped state is subjected to an additional y-dependent potential, such as the V_2 term in Eq. (1), the probability distributions are modulated along the chain length. As long as the excitation gap remains open throughout, time-dependent perturbation theory [adapted to the imaginary-time evolution of Eq. (2)] can be used to evaluate the adiabatic change in the densities of the lines along the y-direction. As we show in the Supplemental Information [27], the instantaneous probability current across the system can be expressed as $J(y) = \frac{1}{L}\partial_y\langle X\rangle$, where crucially $\langle X \rangle$ depends only on the square modulus of the ground-state wavefunction. As a result, the density current is unchanged by the line-fermion mapping $\Psi_0^P = |\Psi_0^F|$ and by the transformation to imaginary time. The shift in the center of mass of the chains over one cycle corresponds exactly to the net shift of electrons belonging to the filled band in the Thouless pump [18, 24],

$$\frac{\langle\Delta x\rangle_\lambda}{a} = \frac{1}{a}\int_0^\lambda J(y)\,dy = \frac{1}{2\pi}\int_0^\lambda dy \int_0^{\frac{2\pi}{a}} dk\,\mathcal{F}(y,k) \equiv \mathcal{C},$$
(3)

where $\mathcal{F}(y,k) = i(\langle\partial_y u_k(y)|\partial_k u_k(y)\rangle - \text{c.c.})$ is the Berry curvature computed using the Bloch eigenstates $|u_k(y)\rangle$ of the lowest band of the Hamiltonian in Eq. (2) with the periodic potential $V(x,y)$ evaluated at a fixed y and $\mathcal{C}$ is the Chern number.

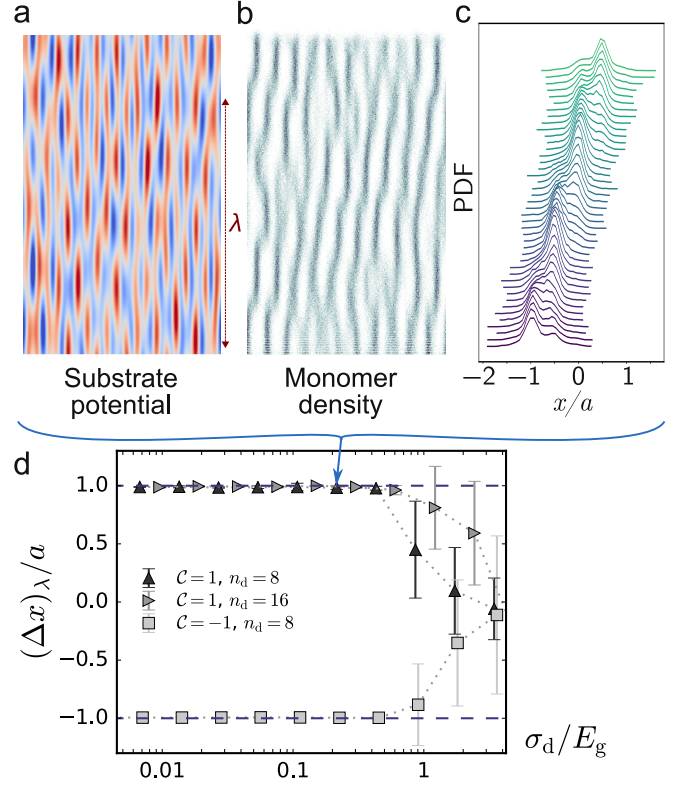Equation (3) establishes the topological origin of the

FIG. 3. **The line tilt is robust against disorder. a,** Example of a substrate potential with $\mathcal{C} = 1$ from Fig. 2a, with random disorder added. **b,** Equilibrium monomer density distribution for potential in **a** under commensurate filling. **c,** Aggregated probability density function of monomer x-positions. Although the density profiles of individual chains show deviations, the aggregated profile maintains the quantized tilt. **d,** Tilt as measured in simulations for increasing disorder added to the substrate interaction for the potentials studied in Fig. 2. Each point represents an average over ten realizations of random disorder; the error bars represent estimated standard deviations. Triangles and squares correspond to underlying periodic potentials with Chern numbers $\mathcal{C} = 1$ and -1 respectively, with n_d additional modes with random amplitude and phase added on. The quantized tilt is preserved until the disorder strength σ_d becomes comparable to the excitation gap E_g.

tilt observed in Fig. 2. The nontrivial mapping between the directed-line and the electronic systems is a physical consequence of two features. First, adiabatic evolution is determined solely by changes in the instantaneous eigenstates of H when the parameter y is changed, and the form of H is preserved exactly on both sides of the mapping. Second, while the Berry curvature is a property of the *complex* eigenstates of the Fourier-transformed Hamiltonian, the Chern number (i.e., integrated Berry curvature) describes the *real*-valued shift in the center of mass of the directed-line probability distribution. Hence, the tilt angle is a physical observable proportional to the Chern number which is analogous to the quantized charge transport of the electronic system.

An important property of topological adiabatic pumps is their robustness against disorder: since the shift in centres of mass of the single-particle states is associated with a topological index, it is unchanged by disorder in the substrate potential as long as the excitation gap between the lowest and higher bands does not close [24]. To test the robustness of the tilt, we add a random noise $V_\mathrm{d}(x,y)$ to the substrate potential (implemented as a superposition of n_d sine functions with random amplitudes and phases, see Methods). Figs. 3a–b show a substrate potential with added disorder, and the corresponding equilibrium monomer density. The density profile in Fig. 3b looks substantially different from its crystalline counterpart in Fig. 2b. In the absence of disorder, the quantized collective shift of all the chains translated to a quantized tilt in the contour of each individual chain; this is no longer true when disorder is present. Nevertheless, the *aggregated* tilt (Fig. 3c) shows a striking regularity. The measured slope of the equilibrium directed-line conformations over one period (Fig. 3d) remains quantized by the Chern number until the disorder strength (the standard deviation σ_d of the disorder potential) becomes comparable to the gap E_g between the occupied band and the next-highest band in the spectrum of $V(x,y)$.

The topological patterning is also robust against general interactions among chains on top of the noncrossing constraint, which translate in the quantum language to many-body interactions (of the same functional form) among the fermions [37]. As with substrate disorder, the quantization is unaffected as long as the excitation gap remains open when the interactions are turned on [24]. This property is demonstrated by the results of our simulations that employ a harmonic contact potential in addition to the noncrossing constraint [27].

The proposed topological phenomenon stands apart from its counterparts in optics and mechanics in several ways. The Chern number manifests itself in a structural property which can be measured directly from the equilibrium pattern. By contrast, in the topological band theory of classical waves, Chern numbers only control the number of chiral edge modes which are typically probed via the transport of energy along the edge. Moreover, to excite an acoustic, optical or mechanical chiral edge mode, the system must be driven at a specific frequency corresponding to the band gap, whereas in the directed-line case there is a notion of band filling, i.e., an effective Fermi level tuned by the chain density. These features could be realized in systems as diverse as colloidomers [38] and magnetic vortex lines in superconducting slabs [39].

_____

* These authors contributed equally to this work.
† vitelli@uchicago.edu

[1] Sebastian D. Huber, "Topological mechanics," Nature Physics **12**, 621–623 (2016).

[2] Roman Süsstrunk and Sebastian D. Huber, "Observation of phononic helical edge states in a mechanical topological insulator," Science **349**, 47–50 (2015).

[3] C. L. Kane and T. C. Lubensky, "Topological boundary modes in isostatic lattices," Nature Physics **10**, 39–45 (2014).

[4] Jayson Paulose, Bryan Gin-ge Chen, and Vincenzo Vitelli, "Topological modes bound to dislocations in mechanical metamaterials," Nat Phys **11**, 153–156 (2015).

[5] Emil Prodan and Camelia Prodan, "Topological phonon modes and their role in dynamic instability of microtubules," Phys. Rev. Lett. **103**, 248101 (2009).

[6] Lisa M Nash, Dustin Kleckner, Alismari Read, Vincenzo Vitelli, Ari M Turner, and William T M Irvine, "Topological mechanics of gyroscopic metamaterials," Proceedings of the National Academy of Sciences **112**, 14495–14500 (2015).

[7] Mikael C Rechtsman, Julia M Zeuner, Yonatan Plotnik, Yaakov Lumer, Daniel Podolsky, Felix Dreisow, Stefan Nolte, Mordechai Segev, and Alexander Szameit, "Photonic Floquet topological insulators." Nature **496**, 196–200 (2013).

[8] Ling Lu, John D Joannopoulos, and Marin Soljačić, "Topological photonics," Nature Photonics **8**, 821–829 (2014).

[9] P.-G. de Gennes, "Soluble model for fibrous structures with steric constraints," Journal of Chemical Physics **48**, 2257–2259 (1968).

[10] P. Le Doussal and D. R. Nelson, "Statistical mechanics of directed polymer melts," EPL (Europhysics Letters) **15**, 161 (1991).

[11] David R Nelson, "Defects and geometry in condensed matter physics," (Cambridge University Press, 2002) Chap. 9.

[12] D. Zeb Rocklin, Shina Tan, and Paul M. Goldbart, "Directed-polymer systems explored via their quantum analogs: Topological constraints and their consequences," Physical Review B **86**, 165421 (2012).

[13] David R. Nelson and V. M. Vinokur, "Boson localization and correlated pinning of superconducting vortex arrays," Physical Review B **48**, 13060–13097 (1993).

[14] Anatoli Polkovnikov, Yariv Kafri, and David R. Nelson, "Vortex pinning by a columnar defect in planar superconductors with point disorder," Physical Review B - Condensed Matter and Materials Physics **71**, 1–11 (2005), arXiv:0409520 [cond-mat].

[15] V. S. Dotsenko, V. B. Geshkenbein, D. A. Gorokhov, and G. Blatter, "Free-energy distribution functions for the randomly forced directed polymer," Phys. Rev. B **82**, 174201 (2010).

[16] Lei Wang, Matthias Troyer, and Xi Dai, "Topological Charge Pumping in a One-Dimensional Optical Lattice," Physical Review Letters **111**, 026802 (2013).

[17] Ran Wei and Erich J Mueller, "Anomalous charge pumping in a one-dimensional optical superlattice," Physical Review A **92**, 013609 (2015).

[18] D. J. Thouless, "Quantization of particle transport," Physical Review B **27**, 6083–6087 (1983).

[19] Shuta Nakajima, Takafumi Tomita, Shintaro Taie, Tomohiro Ichinose, Hideki Ozawa, Lei Wang, Matthias Troyer, and Yoshiro Takahashi, "Topological Thouless pumping of ultracold fermions," Nature Physics **12**, 296–300 (2016).

[20] Michael Lohse, Christian Schweizer, Oded Zilberberg, Monika Aidelsburger, and Immanuel Bloch, "A Thouless quantum pump with ultracold bosonic atoms in an optical superlattice," Nature Physics **12**, 350–354 (2015).

[21] Michael Lohse, Christian Schweizer, Hannah M. Price, Oded Zilberberg, and Immanuel Bloch, "Exploring 4D quantum Hall physics with a 2D topological charge pump," Nature **553**, 55–58 (2018), arXiv:1705.08371.

[22] D. J. Thouless, M. Kohmoto, M. P. Nightingale, and M. den Nijs, "Quantized Hall Conductance in a Two-Dimensional Periodic Potential," Physical Review Letters **49**, 405–408 (1982).

[23] J E Avron, O Kenneth, and G Yehoshua, "A study of the ambiguity in the solutions to the Diophantine equation for Chern numbers," Journal of Physics A: Mathematical and Theoretical **47**, 185202 (2014).

[24] Q Niu and D J Thouless, "Quantised adiabatic charge transport in the presence of substrate disorder and many-body interaction," Journal of Physics A: Mathematical and General **17**, 2453–2462 (1984).

[25] Randall D. Kamien, Pierre Le Doussal, and David R. Nelson, "Theory of directed polymers," Phys. Rev. A **45**, 8727–8750 (1992).

[26] D. Zeb Rocklin and Paul M. Goldbart, "Directed-polymer systems explored via their quantum analogs: General polymer interactions and their consequences,"

Physical Review B **88**, 165417 (2013).

[27] See Supplemental Material at XXXXX for details of simulations and analytical calculations, notes on experimental realizations, Supplemental Figures and Movies, which includes Refs. [28–33]

[28] R. D. King-Smith and David Vanderbilt, "Theory of polarization of crystalline solids," Physical Review B **47**, 1651–1654 (1993).

[29] A. Bruno-Alfonso and D R Nacbar, "Wannier functions of isolated bands in one-dimensional crystals," Physical Review B **75**, 115428 (2007).

[30] Raffaele Resta, "Macroscopic polarization in crystalline dielectrics: the geometric phase approach," Reviews of Modern Physics **66**, 899–915 (1994).

[31] Raffaele Resta, "Quantum-Mechanical Position Operator in Extended Systems," Physical Review Letters **80**, 1800–1803 (1998).

[32] Raffaele Resta, "Manifestations of Berry's phase in molecules and condensed matter," Journal of Physics: Condensed Matter **12**, R107–R143 (2000).

[33] J. Zak, "Berry's phase for energy bands in solids," Physical Review Letters **62**, 2747–2750 (1989).

[34] Sam F Edwards, "The statistical mechanics of polymers with excluded volume," Proceedings of the Physical Society **85**, 613 (1965).

[35] P G De Gennes, "Some conformation problems for long macromolecules," Reports on Progress in Physics **32**, 304 (1969).

[36] Mark W. Matsen, "Self-Consistent Field Theory and Its Applications," in *Soft Matter Vol. 1*, Vol. 1 (Wiley-VCH Verlag GmbH & Co. KGaA, Weinheim, Germany, 2006) pp. 87–178.

[37] M Girardeau, "Relationship between Systems of Impenetrable Bosons and Fermions in One Dimension," Journal of Mathematical Physics **1**, 516 (1960).

[38] Angus McMullen, Miranda Holmes-Cerfon, Francesco Sciortino, Alexander Y. Grosberg, and Jasna Brujic, "Freely jointed polymers made of droplets," Physical Review Letters **121**, 138002 (2018).

[39] C. A. Bolle, V. Aksyuk, F. Pardo, P. L. Gammel, E. Zeldov, E. Bucher, R. Boie, D. J. Bishop, and D. R. Nelson, "Observation of mesoscopic vortex physics using micromechanical oscillators," Nature **399**, 43–46 (1999).